Predicted Changes in Advanced Turboprop Noise with Shaft Angle of Attack

S.L. Padula* and P.J.W. Block†
NASA Langley Research Center, Hampton, Virginia

Current interest in advanced turboprop blade designs and new propeller installation schemes motivated an effort to include unsteady loading effects in an existing propeller noise prediction computer program. The present work validates the prediction capability, while studying the effects of shaft inclination on the radiated sound field. Classical methods of propeller performance analysis supply the time-dependent blade loading needed to calculate noise. Polar plots of the sound pressure level (SPL) of the first four harmonics and the overall SPL are indicative of the change in the directivity pattern as a function of the propeller angle of attack. Noise predictions are compared with newly available wind tunnel data and the accuracy and applicability of the prediction method are discussed. It is concluded that unsteady blade loading caused by inclining the propeller with respect to the flow changes the directionality and intensity of the radiated noise. These changes are well modeled by the present quasisteady prediction method.

Nomenclature

M_t	= rotational tip Mach number
R	= distance from propeller hub to plane defined by microphone locations
r	= distance from propeller hub to a specific microphone
α	= shaft angle of attack
$\beta_{0.75}$	= blade geometric pitch setting at 75% radial station
θ	= polar directivity angle
ϕ	= azimuthal directivity angle

Introduction

THIS paper presents the modifications to the radiated sound field of a propeller caused by inclining the propeller axis with respect to the wind axis. This study was motivated by NASA's interest in advanced turboprop (ATP) propulsion systems for short- and medium-range commuter flights. Past research has established that propeller noise is well predicted if the pressure loading on the blades is known.[1] Measurements of installed propeller noise suggest that unsteady blade loading causes increased noise.[2,3] The intent of this paper is to report on one source of unsteady blade loading and to quantify the change in the sound pressure level as a function of the shaft angle of attack.

It has been established that propeller-driven aircraft usually produce more noise during takeoff than they would in level flight with the same operating conditions.[4] Tests sponsored by the FAA indicate that the maximum A-weighted sound level for a light-aircraft takeoff is about 4 dBA greater than expected based on level flyover measurements for the same aircraft. This excess noise is attributed to the unsteady loading caused by a skewing of the flowfield. The present study investigates the kinematic effects of inclining the shaft axis with respect to the wind axis and estimates the change in the resulting flyover noise.

Presented as Paper 84-2347 at the AIAA/NASA 9th Aeroacoustics Conference, Williamsburg, VA, Oct. 15-17, 1984; submitted Oct. 29, 1984; revision received May 13, 1985. This paper is declared a work of the U.S. Government and therefore is in the public domain.

*Aerospace Engineer.
†Aerospace Engineer, Member AIAA.

The present research constitutes a significant step toward a unified system for predicting ATP noise. All of the prediction techniques used are contained in the NASA Aircraft Noise Prediction Program (ANOPP) and are thoroughly documented in the code itself and elsewhere.[1,5] The value of these prediction methods is greatly enhanced by the existence of a set of high-quality wind tunnel data from the NASA 4×7 m tunnel. Comparisons between data and predictions for a sting-mounted propeller establish the validity of the acoustic model and increase our understanding of the installation effects. The ANOPP acoustic prediction methods are directly applicable to pusher and counter-rotating propellers if the unsteady loading on those blades can be determined.

Analysis Method

Much of the material summarized in this section is covered in greater detail in Refs. 1, 6, and 7. The aim of this section is to explain how existing propeller prediction programs can be modified to include unsteady loading effects. The strengths and limitations of the present methods are discussed.

Classical methods are used to predict the blade loading that varies smoothly with the rotation angle. First, the propeller blade sections are mapped into an elliptical coordinate system and smoothed using cubic splines. The section aerodynamics are computed using Theodorsen's method of successive conformal mapping. Blade element and momentum theory are used to calculate the induced velocity field of the propeller. At first, a uniform inflow is assumed and the induced velocity field is determined for the propeller with no shaft inclination. Then, a simple rotation of the coordinate system models the kinematic effect of the shaft angle of attack. No attempt is made to model the propeller wake or to analyze the effect of the wake on the sound propagation. Once the induced velocities are tabulated as functions of radial distance from the hub and rotational position, the net forces on each blade section as functions of time are easily computed.

The periodic acoustic pressure signature and spectrum of the propeller are calculated using a time-domain solution to the Ffowcs-Williams/Hawkings equation without the quadrupole source term, as derived in Ref. 7. The solution in-

volves a double integral over the actual blade surface and requires detailed geometric and pressure loading information. However, if the net forces on the blade and the blade section areas are known as functions of radial distance, the acoustic equation can be approximated by a single integral over the length of the blade. Essentially, the noise produced by a rotating blade is modeled by a rotating distribution of point sources located at the aerodynamic center of each blade section. This line source approximation is a reliable and efficient alternative to the full-blade formulation for high-aspect-ratio propellers when the helical tip Mach number is less than 0.6 and when the loading is a smooth function of rotation angle.[7] Both the line source approximation and the full-blade formulation are implemented in ANOPP.

It is necessary to modify the acoustic prediction procedures reported in Ref. 1 in order to model a nonzero shaft angle of attack. The simplifying assumption that the propeller moves in a direction parallel to its axis of rotation is not valid. Thus, calculating the position and local velocity of a point on the blade at the emission time requires a new iterative process.

A second modification is required to model the unsteady loading. The net forces on the blade are tabulated as a function of time (or rotation angle). Once the position of the blade at emission time has been calculated, then the loading on the blade and the change in loading with time can be determined by interpolation into the table. For the present work, a spline interpolation procedure was employed. Forces on the blade were tabulated at 20 evenly spaced rotation angles and at 11 spanwise stations. Increasing the number of rotation angles from 20 to 40 or 80 did not significantly change the noise predictions of the first four harmonics.

Figure 1 is a schematic of the polar coordinate system used to calculate and display the propeller noise predictions. The origin of the coordinate system is the center of the propeller hub. The polar angle θ is measured from the shaft axis such that θ is small when the aircraft is approaching an observer location and $\theta = 90$ deg when the aircraft is overhead. The azimuthal angle ϕ is zero beneath the aircraft and is positive in the direction of propeller rotation.

Description of the Experiment and Data Analysis

All of the propeller operating conditions chosen for this study are actual conditions of a recent test of a model-scale four-bladed SR-2 propeller operating at subsonic tip Mach numbers. The entire experiment is described in detail in Ref. 9. The description given below covers those aspects pertaining to the set of data presented herein. The propeller was 0.429 m (16.9 in.) in diameter and was driven by a single 29 hp, 10,000 rpm electric motor.

The nacelle was cylindrical with a maximum outside diameter of 0.15 m (6.0 in.). It was mounted such that it was an aerodynamic extension of the straight sting as shown in Fig. 2a. The straight sting was used to keep the height of the propeller axis 0.889 m (35.0 in.) above the microphone carriage for every configuration.

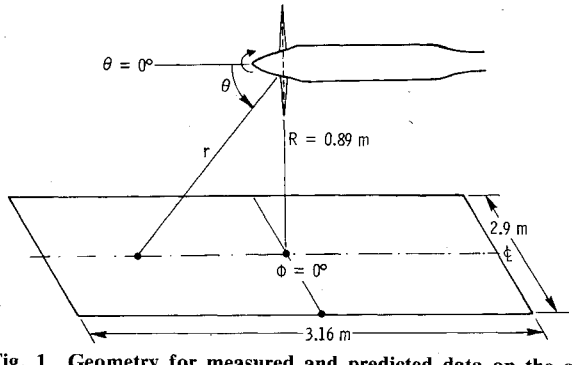

Fig. 1 Geometry for measured and predicted data on the ground plane of all possible microphone positions.

The microphone carriage was a streamlined rectangular flat plate holding an array of 11 flush-mounted microphones (see Fig. 2a). It was designed to circumvent the complexity of reflections from the tunnel floor, while still providing the capability of making numerous streamwise noise measurements of all of the propeller configurations under a very small boundary layer of constant thickness. The carriage was 1.8 m (72 in.) wide (streamwise), 4.27 m (168 in.) long (cross-stream dimension), and 0.0584 m (2.30 in.) thick. It had a rigid foam core and an aluminum skin bonded with an epoxy adhesive. A sketch of the carriage showing the microphone locations is given in Fig. 2b. The carriage was moved in the streamwise

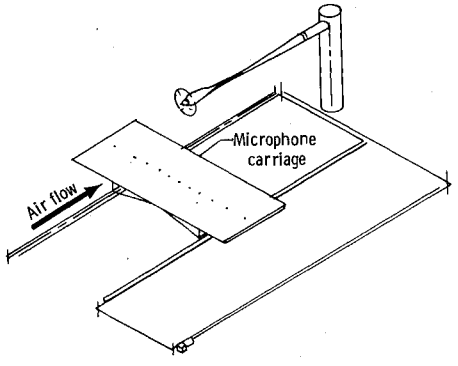

a) Scaled isometric sketch of microphone carriage and propeller.

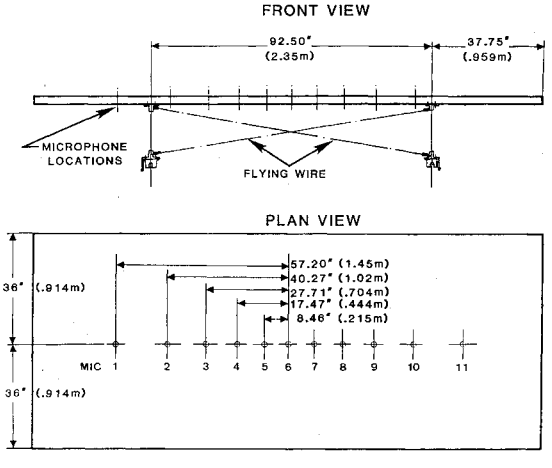

b) Front view and plan view of microphone carriage.

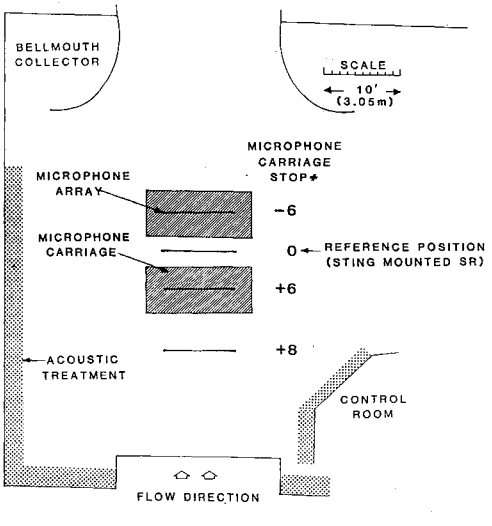

c) Plan view of the Langley 4×7 m tunnel open test section.

Fig. 2 Schematics of experimental apparatus.

direction on Thompson bearings and a set of 1-in.-diam stainless steel rods. The carriage was positioned at 13-15 fixed streamwise locations that corresponded to nominal increments of 10 deg from the propeller disk plane, beginning at 60 deg in front of the disk plane and ending 60 deg behind it. Thus, the noise radiation pattern for each of the propeller configurations was measured at a minimum of 143 locations covering the range of ±60 deg streamwise and about 60 deg laterally.

The tests were conducted in the Langley 4×7 m tunnel. This is a closed, single-return, atmospheric wind tunnel allowing open or closed test section operation. Figure 2c is a plan view scaled drawing of the open test section (OTS) showing the size of the OTS, the size of the microphone carriage, the array of microphones, the propeller plane location, and the locations of the acoustic treatment. The treatment consisted of open-cell foam bats 0.152 m (6 in.) thick applied to the raised ceiling, sidewalls, and control room wall. A tone burst calibration showed that within the dynamic range of the recording instrumentation, the microphone systems were not able to detect reflections from these surfaces.

The microphone data were high-pass filtered at 80 Hz and FM recorded on 1 in. magnetic tape at 60 in./s. A triple-redundancy system was employed for recording the attenuator settings. A 1/rev pulse, which was generated by a magnetic sensor on the shaft, was also recorded. The recorded data were digitized using the 1/rev pulse to obtain 512 points of data for each revolution of the shaft. A minimum of 120 revolutions of data were stored for each microphone (61,440 points) for averaging.

The purpose of the wind tunnel testing was to acquire a set of acoustic data suitable for studying the effects of installation on propeller noise. The tunnel flow velocity was fixed at Mach 0.09, while the blade pitch setting $\beta_{0.75}$, rotational tip Mach number M_t, and shaft angle α were varied. The run numbers and test conditions chosen for the present study are summarized in Table 1.

All of the acoustic data presented in this paper have been ensemble averaged, corrected to the free field, and normalized to a constant radius ($R=0.889$ m), assuming spherical spreading in order to emphasize the installation effects. The mean signal was computed by averaging the sampled acoustic signal over 120 shaft revolutions. The mean signal is always plotted as confidence bands, indicating one standard deviation on each side of the mean. The Fourier coefficients of the sampled signal are also averaged over 120 revolutions and then converted to sound pressure levels for plotting. The sound levels obtained for the flush-mounted microphones are corrected to free-field levels by subtracting 6.02 dB. Finally, the sound pressure levels computed for each microphone position have been corrected for spherical spreading by adding $20\log(r/R)$, where R is the distance from the hub to the ground plane and r the distance from the hub to the microphone (recall Fig. 1). This treatment of the data highlights the effect of shaft angle changes and suppresses the effect of spherical spreading and random fluctuations.

Results and Discussion

In this section, measured and predicted noise levels are compared both to validate the prediction methods and to explain the acoustic radiation patterns observed in the wind tunnel test. Time history and spectral plots are used to justify the approximate formulations and the numerical techniques used to predict noise. Contour plots of noise levels on the conceptual ground plane indicate the extent to which the physical phenomena are modeled by the theory. Finally, polar plots of the overall sound pressure levels clearly show the predicted change in the directivity pattern as a function of the propeller shaft angle of attack.

Table 1 Summary of test conditions

Run	$\beta_{0.75}$, deg	M_t	α, deg
55	12.7	0.76	0
52	20.6	0.40	0
63	20.6	0.40	8
65	20.6	0.40	−8

Assessment of Acoustic Prediction Methods

The comparison between the measured and predicted data is examined for two different run conditions at zero angle of attack. Run 55 represents the highest propeller tip Mach number ($M_t=0.76$) tested. A high rotational speed is advantageous because the propeller produces noise levels well above the background levels in the tunnel. It is troublesome because the lifting line theory used to predict the performance and line source approximation used to predict the acoustic radiation degrade as the tip Mach number is increased. On the other hand, run 52 represents the lowest tip Mach number tested

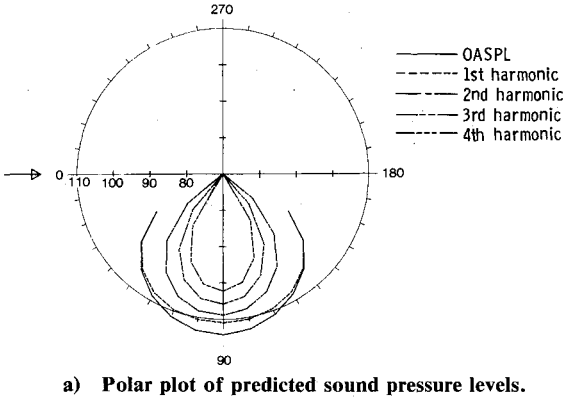

a) Polar plot of predicted sound pressure levels.

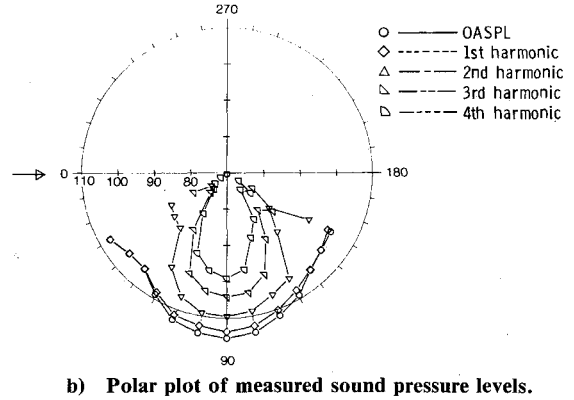

b) Polar plot of measured sound pressure levels.

Fig. 3 Noise directivity pattern for run 55 ($\beta_{0.75}=12.7$ deg, $M_t=0.76$, $\phi=0$ deg, $r=0.89$ m).

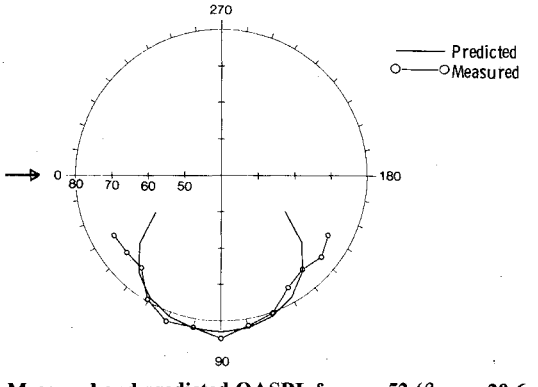

Fig. 4 Measured and predicted OASPL for run 52 ($\beta_{0.75}=20.6$ deg, $M_t=0.40$, $\phi=0$ deg, $r=0.89$ m).

($M_t = 0.40$). The theory should model this run quite well—as long as the low-level propeller noise can be distinguished from other noise sources.

Figure 3a is a polar plot of the noise directivity pattern predicted for run 55. The solid curve is a plot of overall sound pressure level (OASPL) as a function of θ, where θ is the polar angle measured from the propeller shaft axis. The dashed lines indicate the predicted levels for the first four harmonics. Figure 3b shows the corresponding measured data from run 55. Data recorded by the microphone at the center of the movable carriage have been corrected to free-field values at a constant radius of 0.889 m. The measured and predicted directivity patterns are very similar except at $\theta = 30$ and 150 deg. If these two extreme points are excluded, the average difference between measured and predicted OASPL in these plots is 1.4 dB. Notice that the harmonic levels in Fig. 3 compare about as well as the overall levels. Figure 4 is a polar plot of the measured and predicted OASPLs for run 52. Notice that the levels plotted here are greatly reduced from those plotted for run 55, and that the comparison between measured and predicted levels is good.

Figure 5 compares the measured and predicted signals at a single microphone location. The microphone directly under the propeller is selected so that no correction for spherical spreading is required. In each plot, the heavy solid line represents the predicted signal and the thin line the signal reconstructed from the average Fourier coefficients. The shaded band shows the scatter in the data around the mean signal. Figure 5a contains the signal produced by one revolution of the propeller in run 55 and Fig. 5b is a similar time history plot for run 52. In both cases, the predicted signal models the measured signal quite well.

A few words must be said about the numerical stability and repeatability of the predictions contained herein. The authors conducted a number of numerical experiments to determine whether small changes in the input would cause noticeable differences in the published plots. The predictions proved to be extremely stable with respect to the number of time points used to calculate the spectrum and to the particular grid used to represent the blade shape. Likewise, small changes in the tip speed, forward velocity, pitch setting, or other input quantities made only negligible changes in the predicted signal.

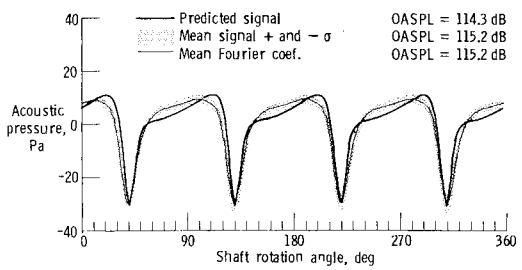

a) Signal for run 55 at $\theta = 90$ deg and $\phi = 0$ deg.

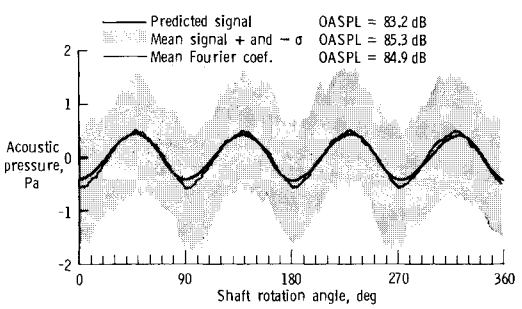

b) Signal for run 52 at $\theta = 90$ deg and $\phi = 0$ deg.

Fig. 5 Measured and predicted acoustic signal.

Finally, the use of the line source approximation rather than the full-blade formulation caused no change in the published results, but reduced the cost of the numerous computer runs by a factor of 10.

The only problems encountered in preparing this report involved the prediction of propeller noise near the shaft axis. Theoretically, thickness and periodic loading noise diminish rapidly as θ approaches zero. If the inflow is perfectly uniform and the four blades are identical and evenly spaced in the hub, then the signals arriving from each blade will cancel one another along the shaft axis. Any asymmetry in the problem, such as a nonzero shaft angle of attack, will interfere with this cancellation. Thus, the effects of the shaft angle of attack should be most pronounced near the axis of the propeller ($\theta = 0$ deg). As a practical matter, however, propeller noise predictions near the axis are avoided. For one thing, noise levels in this direction are seldom significant for either flyover or interior noise estimates. Moreover, since the flow is never perfectly uniform nor the blades perfectly made, the predicted cancellation effects near the shaft axis have little practical significance. Finally, since the signal from each blade is equally important, small computational errors tend to be multiplied by the number of blades. Thus, in this report, predictions are computed and plotted for polar angles between 30 and 150 deg.

Contour Plots of Noise Directivity Patterns

The effects of shaft angle of attack are illustrated through contour plots of measured and predicted overall sound pressure levels. Contour plots over the plane described by all possible microphone locations indicate that unsteady loading does cause noticeable changes in the intensity and directionality of the radiated noise. Corresponding plots of the predicted OASPL indicate that the observed changes in the data can be

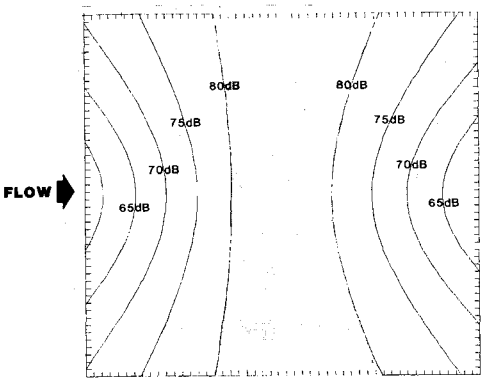

a) Predicted levels corrected to $r = 0.89$ m.

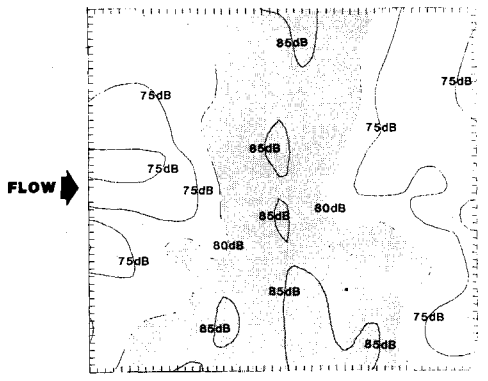

b) Measured levels corrected to $r = 0.89$ m.

Fig. 6 OASPL contours over all microphone locations for run 52 at 0 deg angle of attack.

explained by the theory. Runs 52, 63, and 65 ($\alpha = 0$, $+8$, and -8, respectively) were studied because the angle-of-attack effects are the most pronounced for this set of operating conditions. Run 55 and its corresponding nonzero angle-of-attack runs are not presented because these runs are dominated by thickness noise and show little change with unsteady loading.

The noise radiation pattern for the selected configurations is presented in line contour plots with 5 dB intervals. Thus, these plots present the data corrected to the free field, normalized to constant radius, and then displayed on the grid defined by the 143 microphone locations. To achieve a smooth representation for the contour plots, the 143 measurements were fit with a two-dimensional cubic spline having zero tension. Additional interpolated values were then calculated and the matrix of data was enriched from 11 (microphones) $\times 13$ (streamwise stops) to a 50×50 matrix of evenly spaced points. These 50 points are indicated in the frame of the line contour plots.

Figure 6 shows contour plots of measured and predicted OASPLs for run 52. Here the propeller is directed straight into the flow and is positioned above the center of the plane swept out by the microphone carriage. Areas of the plane where the predicted levels exceed 80 dB are shaded to help the reader compare one plot with another. Since propeller noise is axisymmetric about the prop axis and since the OASPLs are corrected for spherical spreading, the predicted levels in Fig. 6a follow the lines of constant θ on the ground plane (recall Fig. 1). The contour plot of the measured data, shown in Fig. 6b, lacks the symmetry of the predicted plot and the levels are slightly higher than predicted. Apparently, there is a source of noise present in the tunnel tests that is not modeled by the theory. Possible explanations for the excess noise include contamination of the signal by background noise levels in the tunnel, extra source noise because nonuniform inflow conditions cause unsteady loading on the propeller, or extra noise radiated from the vibrating sting mounting system. The lack of symmetry in the measured data may be due to the aforementioned causes or may indicate that the sound has been scattered because of the presence of a large sting behind the propeller.

The effects of the shaft angle of attack are clearly demonstrated by comparing Fig. 6 with Figs. 7 and 8. Figure 7 contains contour plots for run 63. This run is very similar to run 52 except that the propeller shaft is rotated up 8 deg from the horizontal. Notice that the measured and predicted levels now compare reasonably well. Also note that the shaded region denoting noise levels above 80 dB is considerably larger in Fig. 7 than in Fig. 6. This indicates that the unsteady loading on the propeller due to a positive shaft inclination angle causes increased noise levels on the ground. Finally, Fig. 8 contains a set of contour plots for run 65. Here the propeller is rotated down 8 deg from the horizontal. Once again, the measured and predicted patterns are similar. Note also that a negative shaft angle causes a marked decrease in noise levels.

Predicted Effects of Shaft Angle of Attack

It is evident from all of the comparisons of the measured and predicted data that the theory consistently models trends and adequately predicts the levels observed in the data. In this subsection, polar plots of the predicted sound pressure levels are examined to gain further understanding of the effect of unsteady loading on noise. The operating conditions used in this subsection are based on run 63; however, the angles of attack studied and the directivity patterns plotted need not be limited to test conditions.

Figure 9 contains polar plots of run 63 at gradually increasing values of the shaft angle of attack. In these plots, the flow direction, indicated by an arrow, is changing while the shaft axis ($\theta = 0$ deg) remains horizontal. The directivity patterns of the OASPLs plus the fundamental, second, third, and fourth harmonics are plotted for polar angles between 30 and 150 deg

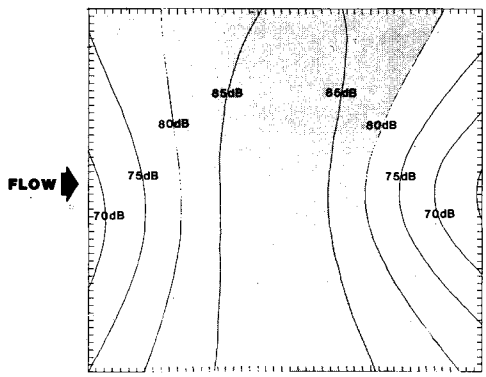

a) Predicted levels corrected to $r = 0.89$ m.

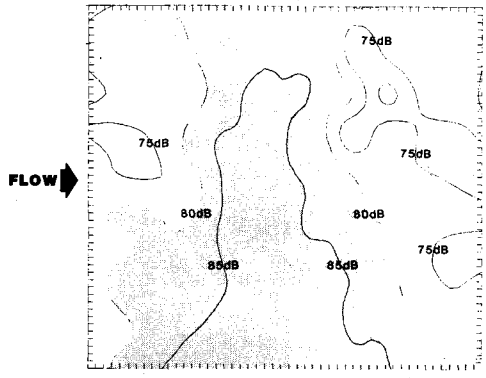

b) Measured levels corrected to $r = 0.89$ m.

Fig. 7 OASPL contours over all microphone locations for run 63 at $+8$ deg angle of attack.

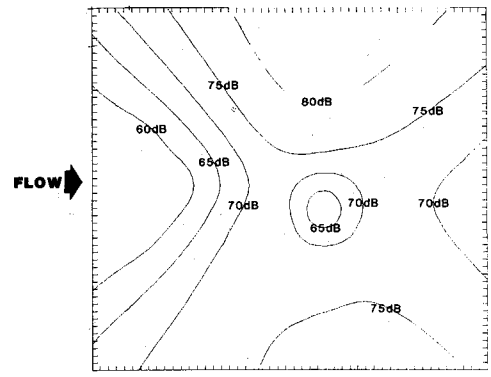

a) Predicted levels corrected to $r = 0.89$ m.

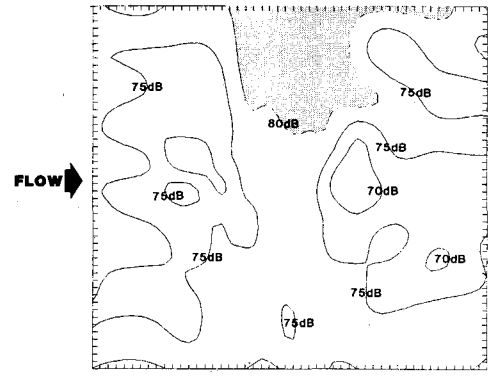

b) Measured levels corrected to $r = 0.89$ m.

Fig. 8 OASPL contours over all microphone locations for run 65 at -8 deg angle of attack.

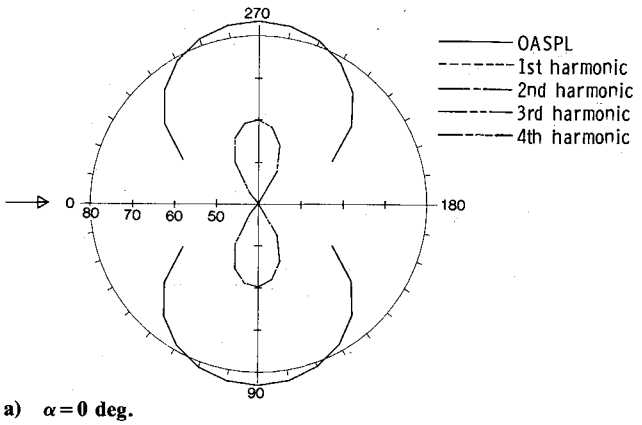

a) $\alpha = 0$ deg.

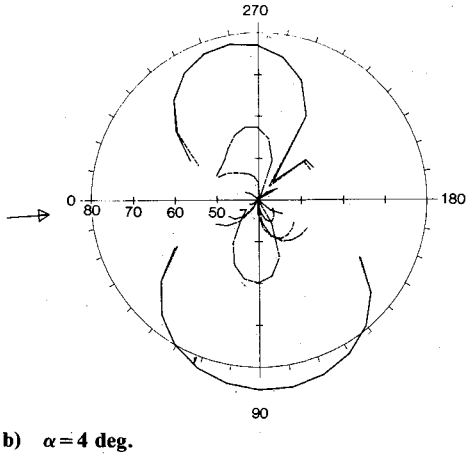

b) $\alpha = 4$ deg.

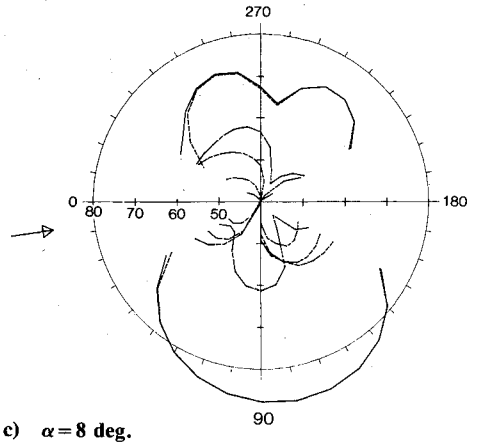

c) $\alpha = 8$ deg.

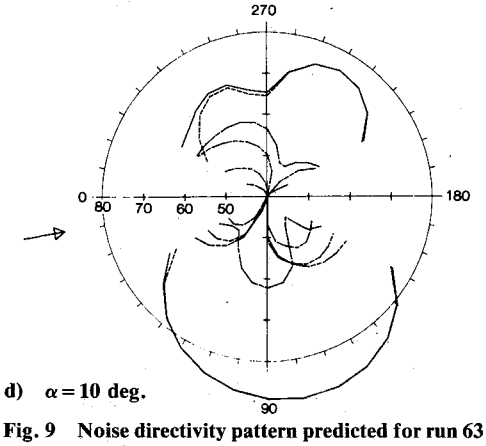

d) $\alpha = 10$ deg.

Fig. 9 Noise directivity pattern predicted for run 63 ($\beta_{0.75} = 20.6$ deg, $M_t = 0.40$, $r = 0.89$ m, $\phi = 0$ deg).

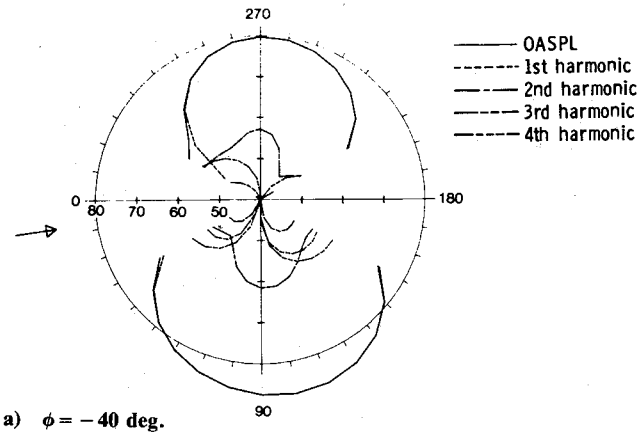

a) $\phi = -40$ deg.

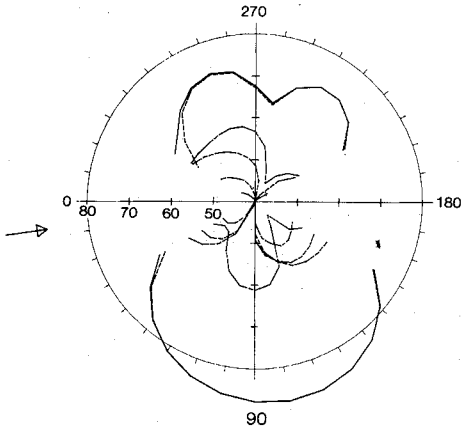

b) $\phi = 0$ deg.

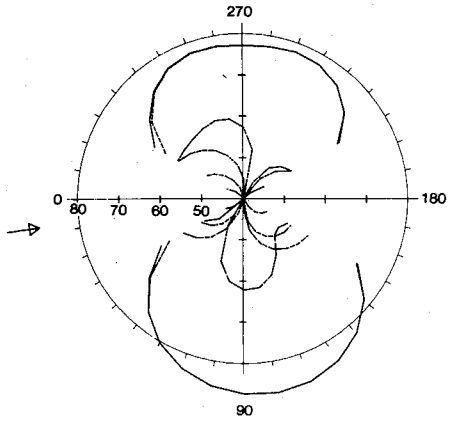

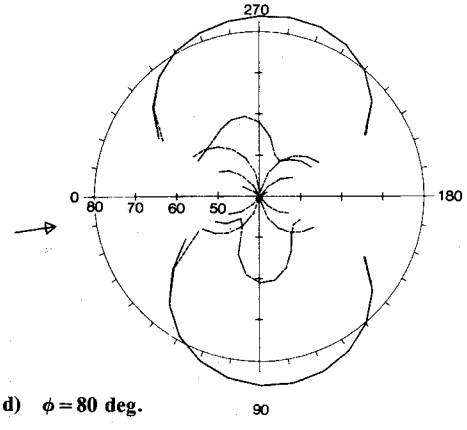

d) $\phi = 80$ deg.

Fig. 10 Noise directivity pattern predicted for run 63 ($\beta_{0.75} = 20.6$ deg, $M_t = 0.40$, $r = 0.89$ m, $\alpha = 8$ deg).

and between 210 and 330 deg from the shaft axis. Thus, the effects previously attributed to positive and negative shaft inclination angles are manifested on a single plot. Comparing Figs. 9a-d, observe that the OASPL is determined almost completely by the first harmonic levels. As the angle of attack increases from one plot to the next, the first harmonic levels increase on the lower half of the plots and decrease on the upper half—as expected. On the other hand, the higher harmonics tend to increase in every direction as the angle of attack increases.

All of the plots in Fig. 9 are calculated for an azimuthal angle ϕ of 0 deg. Numerous predictions at a variety of azimuthal angles indicate that the greatest effects of the shaft angle of attack occur when $\phi = 0$ deg. Figure 10, for instance, compares plots of the OASPLs for run 63 at azimuthal angles of -40, 0, 40, and 80 deg. Notice that the effects of unsteady loading are less and less obvious as ϕ approaches ± 90 deg. At first glance, this result seems to contradict the fact that the blade loading and blade local velocities are maximized at $\phi = -90$ deg. However, the noise is proportional to the components of loading and velocity *in the direction of the observer*. When the blade is at -90 deg (i.e., parallel to the right wing), it is moving toward the observer locations on the ground. Consequently, noise near the ground track of the flight path increases, while noise above the aircraft decreases.

Implications for Flyover Noise Prediction

Since propellers are designed and installed to have no shaft angle of attack in normal cruise conditions, the present work is especially important for predictions of takeoff and landing noise. Figure 11 compares the predicted OASPL values for run 63 with those of run 52. The difference between these two plots is indicative of the error that could be made if takeoff effective perceived noise levels (EPNL) were estimated without accounting for the unsteady loading on the propeller.

Unsteady loading will have either an adverse or a beneficial effect on takeoff noise levels, depending on the installation of the propeller. A tractor mounted on the wing or the nose of the aircraft will have a positive shaft inclination angle during takeoff and will produce excess noise on the ground. On the other hand, if the same tractor propeller is mounted near the tail, it could experience negative shaft inclination angles due to the increased downwash from the wing on takeoff. Such a propeller could produce lower than expected noise on the ground.

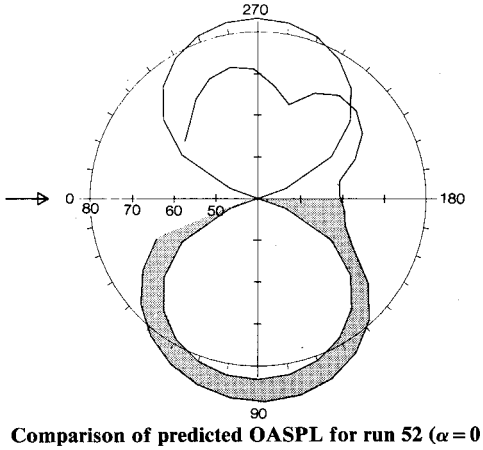

Fig. 11 Comparison of predicted OASPL for run 52 ($\alpha = 0$ deg) and run 63 ($\alpha = 8$ deg).

Shaft inclination angle is not always an important parameter in predicting propeller noise. Some advanced turboprop propulsion systems may have tip Mach numbers and disk loadings such that thickness noise is the dominant noise source even during takeoff. The noise radiation pattern of such a propeller is not sensitive to shaft inclination angle. Likewise, pusher or counter-rotating propellers will not be sensitive to the shaft angle because these configurations have other, more important sources of unsteady loading noise. The current technique could be extended to provide propeller noise prediction methods for pusher and counter-rotating propellers.

Conclusions

It is concluded that unsteady blade loading caused by inclining the propeller with respect to the flow direction significantly modifies the radiated sound field. The angle-of-attack effect can be modeled by modifying existing prediction codes. The validity of these predictions is confirmed by comparison with high-quality wind tunnel data. These findings impact future prediction of propeller noise, particularly if the predicted source noise is used to estimate takeoff and landing perceived noise levels or interior noise levels. The numerical techniques that proved to be effective in this study can be extended to other cases of propellers operating in nonuniform flowfields. Pusher propellers operating in the wake of a wing or strut are one example. With modified performance calculations, even counter-rotating propeller noise can be studied using the present approach.

References

[1]Padula, S. L. and Block, P. J. W., "Acoustic Prediction Methods for the NASA Generalized Advanced Propeller Analysis System (GAPAS)," AIAA Paper 84-2243, July 1984.

[2]Block, P. J. W. and Martin, R. M., "Results from Performance and Noise Tests of Model Scale Propellers," SAE Paper 830730, April 1983.

[3]Tanna, H. K., Burrin, R. H., and Plumblee, H. E., Jr., "Installation Effects on Propeller Noise," *Journal of Aircraft,* Vol. 18, April 1981, pp. 303-309.

[4]International Civil Aviation Organization (ICAO), "Stringency of a Takeoff Standard for Light Propeller-Driven Aeroplanes," Working Paper CAN/7-WP/48 presented by J. E. Wesler, USA, Committee on Aircraft Noise (CAN) at Seventh Meeting, Montreal, May 1983.

[5]Farassat, F., "Linear Acoustic Formulas for Calculation of Rotating Blade Noise," *AIAA Journal,* Vol. 19, Sept. 1981, pp. 1122-1130.

[6]Zorumski, W. E., "Propeller Noise Prediction," NASA TM-85636, May 1983.

[7]Farassat, F. and Succi, G. P., "The Prediction of Helicopter Rotor Discrete Frequency Noise," *Vertica,* Vol. 7, No. 4, 1983, pp. 309-320.

[8]Block, P. J. W., "The Effects of Installation on Single- and Counter-Rotation Noise," AIAA Paper 84-2263, Oct. 1984.

[9]Block, P. J. W., "Installation Noise Measurements of Model SR and CR Propellers," NASA TM-85790, May 1984.